Characterization of Atomic Layer Deposited WN_xC_y Thin Film as a Diffusion Barrier for Copper Metallization

Soo-Hyun Kim, Su Suk Oh, Hyun-Mi Kim, Dae-Hwan Kang[1], Ki-Bum Kim, Wei-Min Li[2], Suvi Haukka[2], and Marko Tuominen[2]
School of Materials Science and Engineering, Seoul National University, Seoul 151-742, Korea
[1]Research Institute of Advanced Materials, Seoul National University, Seoul 151-742, Korea
[2]ASM Microchemisty Ltd., FIN-02631 Espoo, Finland

ABSTRACT

The film properties of WN_xC_y films deposited by atomic layer deposition (ALD) using WF_6, NH_3, and triethylboron source gases were characterized as diffusion barrier for Cu metallization. It is noted that the as-deposited film shows an extremely low resistivity of about 350 μΩ-cm with a film density of 15.37 g/cm^3. The film composition measured from Rutherford backscattering spectrometry shows W, C, and N of approximately 48, 32, and 20 at.%, respectively. Transmission electron microscopy analyses show that the as-deposited film is composed of face-centered-cubic phase with a lattice parameter similar to both β-WC_{1-x} and β-W_2N with an equiaxed microstructure. The barrier property of this ALD-WN_xC_y film at a nominal thickness of 12 nm deposited between Cu and Si fails only after annealing at 700 °C for 30 minutes while the sputter-deposited Ta (12 nm) and ALD-TiN (20 nm) fail at 650 and 600 °C, respectively. It is thought that the superior diffusion barrier performance of ALD-WN_xC_y film is the consequence of both nanocrystalline equiaxed grain structure and the formation of high density film.

INTRODUCTION

Atomic layer deposition (ALD) is being increasingly used to deposit extremely thin films used in semiconductor devices. Since this process is mainly relying on a chemisorption and surface reaction by the sequential delivery of source gases, this technique has the advantages of depositing uniform thin film layer with controlled stoichiometry and an extremely conformal film [1, 2]. Because of these advantages, ALD process is being considered as a promising process technique to deposit future generations of barrier layers, gate dielectrics, and high-*k* dielectrics. Still, however, it is not clear whether the films deposited by ALD process will meet the film qualities of each application as compared to those deposited by other film deposition techniques.

One major application of ALD process is the diffusion barrier layer since this layer requires a conformal deposition down to less than 5 nm in thickness. In this reason, many transition metal nitrides have been deposited by ALD process in order to develop a suitable diffusion barrier for Cu metallization [3-13]. For instance, ALD-TiN film with low resistivity (~200 μΩ-cm), extremely good step coverage, and low Cl content (< 2 at.%) could be obtained by ALD process [5]. However, the use of $TiCl_4$ and NH_3 is known to bring about the Cu pitting when TiN film is deposited directly on Cu surface as a result of Cl-containing by-product [5]. In addition, the barrier properties of this TiN film are not good enough due to the formation of columnar grain structure, which provides the easy pathway for Cu migration. In the case of ALD-TaN process, the formation of high resistivity Ta_3N_5 (~200 Ω-cm) instead of the metallic TaN is known to one of the major problems when $TaCl_5$ and NH_3 were used as source gases. Metallic TaN film could be deposited by the additional Zn pulse [7] or using plasma-enhanced ALD process [11]. Still, however, the resistivity of ALD-TaN film was quite high as about 900 μΩ-cm [7] or as about 1680 μΩ-cm [11] and the barrier properties of these materials against Cu metallization was not reported. ALD-WN_x [5, 10] film was also deposited using sequential supplies of WF_6 and NH_3 at 350 °C but it also suffered from a high resistivity (~4500 μΩ-cm and even higher).

Recently, it has been reported that ALD-WN_xC_y can be deposited with an excellent resistivity of about 350 μΩ-cm [12, 13]. Considering the inherent advantages of ALD process, this material can be utilized as a new diffusion barrier for Cu metallization only if the barrier property is guaranteed. In this report, we will report the film properties and demonstrate that the barrier property of this material is indeed far superior to other materials reported so far.

EXPERIMENTS

ALD-WN_xC_y films of different thickness were deposited onto Si or 20-nm-thick thermally grown SiO_2 using a Pulsar®2000 standalone ALCVD™ reactor module using WF_6, NH_3, and triethyl boron (TEB) as chemical precursors. The detailed descriptions of deposition conditions are reported in the previous publication [12]. Rutherford backscattering spectrometry (RBS) was used for the quantitative analysis of film composition and film density using RUMP simulation program [14]. Transmission electron microscopy (TEM, JEM-3000F) was used for the microstructure and phase analysis. The diffusion barrier performance of 12-nm-thick ALD-WN_xC_y film was evaluated between Cu and Si after annealing in high vacuum ($< 5\times10^{-5}$ Torr) for 30 minutes using sheet resistance measurements, x-ray diffractometry (XRD), and etch-pit test after Secco etching. For comparison, the diffusion barrier performance of the sputter-deposited Ta (12 nm) and ALD-TiN (20 nm) film was also evaluated.

RESULTS AND DISCUSSIONS

A. Properties of ALD-WN_xC_y film

Composition and Density

Figure 1 shows the RBS spectra of WN_xC_y film (~24 nm) deposited on Si substrate. When the incident energy of He^{++} is 2 MeV as shown in Fig. 1(a), one can hardly observe any backscattering signals from carbon and nitrogen even though Auger electron spectroscopy (AES) analysis shows a considerable amount of them [15]. This result is due to the low kinematic factors and the low scattering cross-sections of light elements [16]. However, when the incident He^{++} energy is 3.694 MeV [Fig. 1(b)], backscattering signals from C and N are clearly shown. Using RUMP simulation program, the quantitative film composition is determined to be 48 at.% of W, 32 at.% of C, and 20 at.% of N. Surprisingly, impurities such as F, B, and O in the film are not detected by AES indicating that the reduction process of WF_6 with TEB occurs cleanly on the surface and also the film density is high enough to prevent any oxygen penetration in the film. Film density of 15.37 g/cm^3 was calculated considering the areal density simulated by RUMP program and the film thickness determined by cross-sectional TEM (XTEM) analysis. As compared to the calculated bulk density values of tungsten carbides and tungsten nitrides (W_2C, W_2N, WC, and WN), this film has a relatively high density, corresponding to more than ~90% of bulk values. Obtaining this high density of film by the ALD process should be considered as quite a surprising result considering the low deposition temperature and provides a good clue to think that the barrier property of this film will be quite good [17].

Phase and Microstructure of the as-deposited film

The plan-view TEM bright-field (BF) image of WN_xC_y film (~24 nm) shows very fine granular-like grains and it is very difficult to identify the grain boundaries [Fig. 2(a)]. Dark-field (DF) image [Fig. 2(b)] obtained by placing an objective aperture on the first-order ring of the diffraction pattern [Fig. 2(c)] clearly shows that WN_xC_y film is mainly composed of nanocrystals with the size of 3~7 nm. Selected area electron diffraction pattern also indicates that the film is not amorphous but crystalline. Moreover, a careful comparison of the electron diffraction pattern

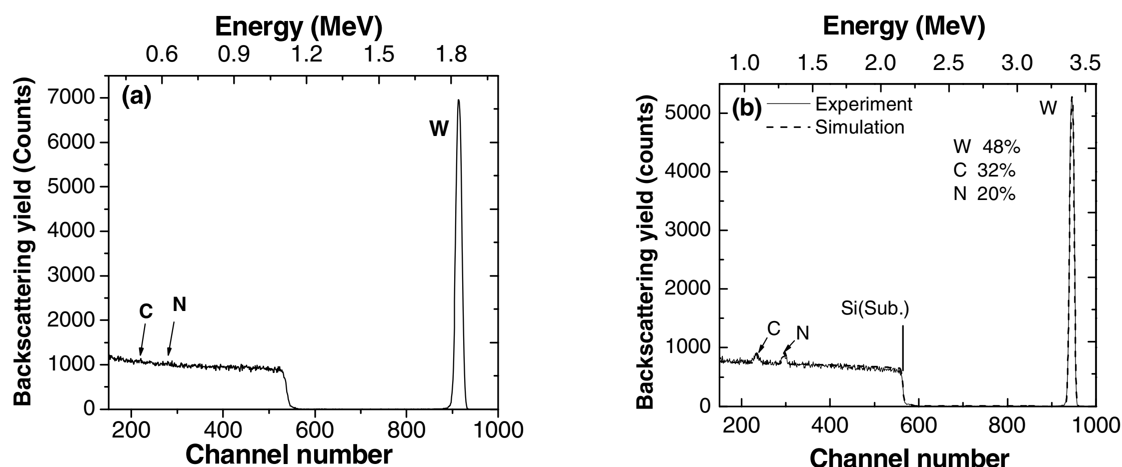

Figure 1. RBS spectra of ALD-WN_xC_y film deposited on Si substrate at 313 ºC when the incident energy of He^{++} is (a) 2 MeV and (b) 3.694 MeV.

with those of W-related materials (W_2C, W_2N, WC_{1-x}, WC, and WN) reveals that the diffraction pattern is well matched with that of β-WC_{1-x} [Cubic, space group: *Fm3m*] or β-W_2N [Cubic, space group: *Pm3m*]. The clear distinction between these two phases is problematic since both of these phases have the same crystal structure [rock salt structure where W atom is located at a face-centered-cubic (fcc) lattice and N or C atom is located at its octahedral sites] and very similar lattice parameter (β-WC_{1-x}: 4.236 Å, β-W_2N: 4.126 Å). High-resolution TEM (HRTEM) image [Fig. 2(d)] also shows the nanocrystals with the size of a few nanometers. We identified that the lattice fringe spacing of grains in the HRTEM images to be about 2.39 and 2.08 Å, which are very close to those of fcc β-WC_{1-x} (111) (d=2.43 Å) or fcc β-W_2N (111) (d=2.38 Å) and fcc β-WC_{1-x} (200) (d=2.11 Å) or fcc β-W_2N (200) (d=2.06 Å). Figure 3 shows the XTEM images of WN_xC_y film (~24 nm) deposited on Si. The dark-field image [Fig. 3(b)] reveals the equiaxed grains with the size of a few nanometers. Although the origin of this kinds of microstructure formation during the ALD process is still not clear, there is no doubt that this equiaxed microstructure is better than that of the columnar in preventing Cu diffusion. High-resolution image also shows the nanocrystalline equiaxed microstructure with densely packed grains [Fig. 3(c)].

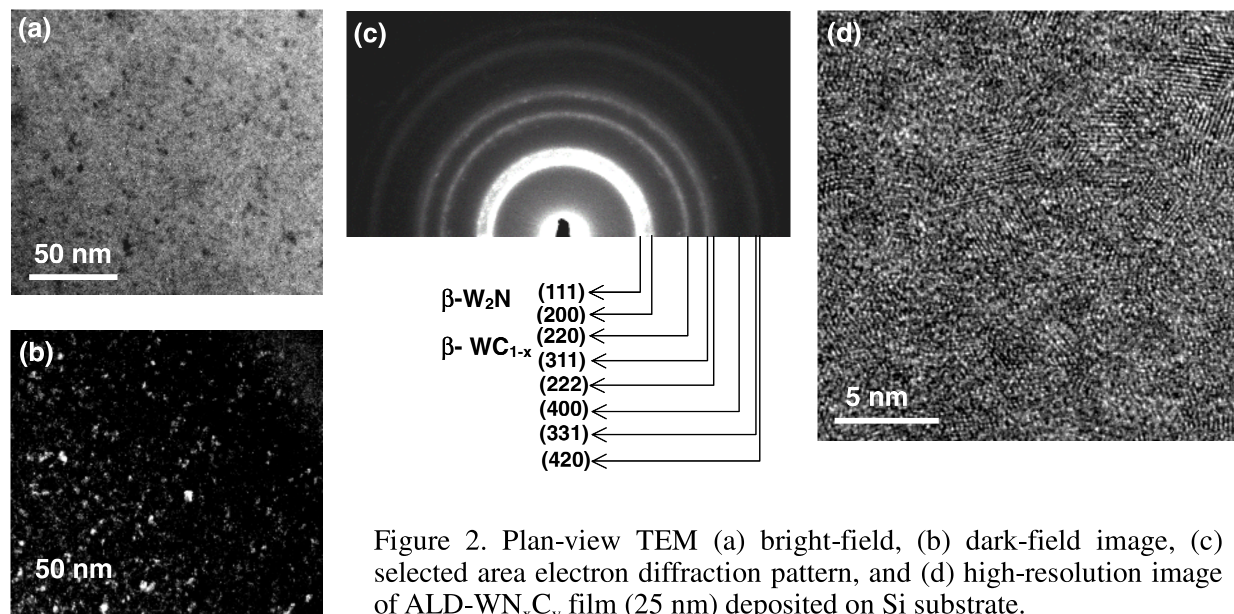

Figure 2. Plan-view TEM (a) bright-field, (b) dark-field image, (c) selected area electron diffraction pattern, and (d) high-resolution image of ALD-WN_xC_y film (25 nm) deposited on Si substrate.

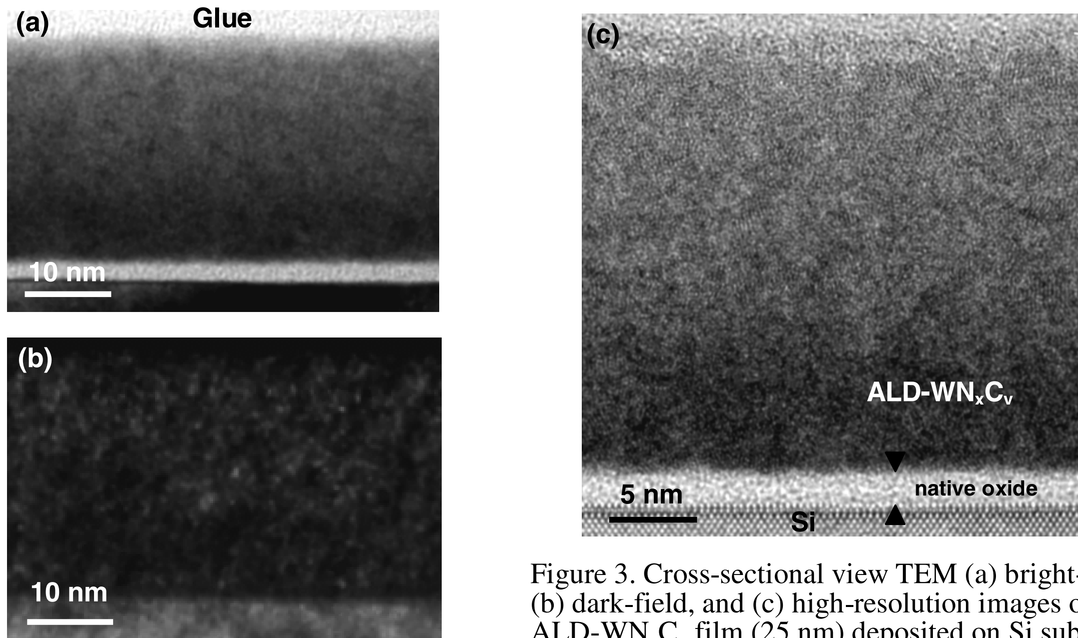

Figure 3. Cross-sectional view TEM (a) bright-field, (b) dark-field, and (c) high-resolution images of ALD-WN_xC_y film (25 nm) deposited on Si substrate.

B. Diffusion Barrier Properties of ALD-WN_xC_y film against Cu

Sheet resistance measurements

Figure 4 shows the changes in sheet resistance of Cu/ALD-WN_xC_y (12 nm)/Si, Cu/sputter-deposited Ta (12 nm)/Si, and Cu/ALD-TiN (20 nm)/Si structures as a function of annealing temperature. The sheet resistance of Cu/WN_xC_y/Si structure starts to increase after annealing at 700 ºC. In the case of Cu/Ta/Si structure, the first increase in sheet resistance is observed after annealing at 650 ºC, which is 50 ^oC lower than that in Cu/WN_xC_y/Si sample. For Cu/TiN/Si structure, the first increase in sheet resistance starts at 600 ºC although the barrier thickness is almost twice thicker than that of WN_xC_y film. It is to be noted that, in all Cu/barrier/Si structures, the temperatures where the sheet resistance starts to increase are the same as the temperatures where copper silicide formation is first observed by XRD (not shown here). This indicates that the increase in sheet resistance is caused by the loss of Cu due to copper silicide formation.

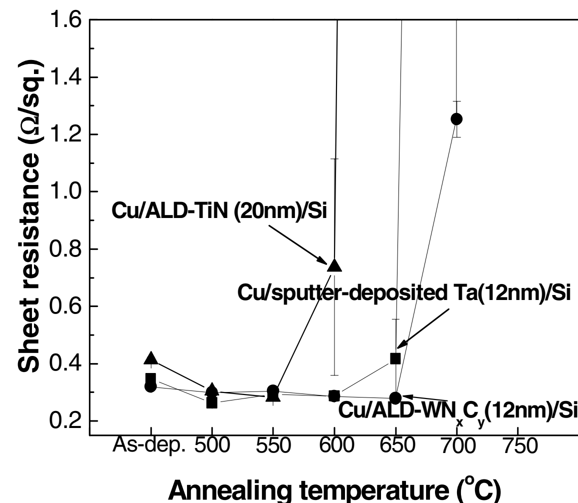

Figure 4. Sheet resistance changes of Cu/ALD-WN_xC_y (12 nm)/Si, Cu/sputter-deposited Ta (12nm)/Si, and Cu/ALD-TiN (20nm)/Si structures as a function of annealing temperature.

Etch-pit test

It is to be noted that sheet resistance measurements and XRD are not sensitive enough for the trace amount of Cu-Si compound, which can be formed on Si surface at the onset of barrier failure. Therefore, the more sensitive etch-pit test was performed. Si surface was

observed under a scanning electron microscope (SEM) after a brief Secco-etch. In fact, regarding the barrier failure in Cu/barrier/Si system, etch-pit test has been known to show better accuracy than sheet resistance measurement and XRD. According to this test, the etch pit was first observed on Si surface at 600 ^{o}C, for Cu/WN_xC_y/Si sample. This temperature is 100 ^{o}C lower than those where the sheet resistance first increased and copper silicide first observed in XRD. As the annealing temperature increased to 650 ^{o}C, the density and size of etch-pits increased. Similarly, etch pits were first observed at 550 ^{o}C for the Cu/Ta/Si sample and at 500 ^{o}C for the Cu/ALD-TiN/Si, respectively. The typical micrographs showing etch pits on the Si surface are represented in figures 5(a)-(c).

These results thus demonstrate that the ALD-WN_xC_y film shows the superior barrier property against Cu migration as compared to those of sputter-deposited Ta and ALD-TiN films. Undoubtedly, the superior barrier performance of this film is the consequence of both high density and non-columnar grain structure. Considering the inherent advantages of the ALD process in obtaining superior conformal deposition, the demonstration of this better barrier property of ALD-WN_xC_y for blanket films guarantees the better application of this film in an actual device structures [18]. In addition, this advantage of ALD-WN_xC_y film is likely to be more significant as the device size shrinks. Table I shows the failure temperatures of various kinds of Cu diffusion barriers determined by XRD, indicating that ALD-WN_xC_y film is one of the best diffusion barriers against Cu considering its very thin thickness.

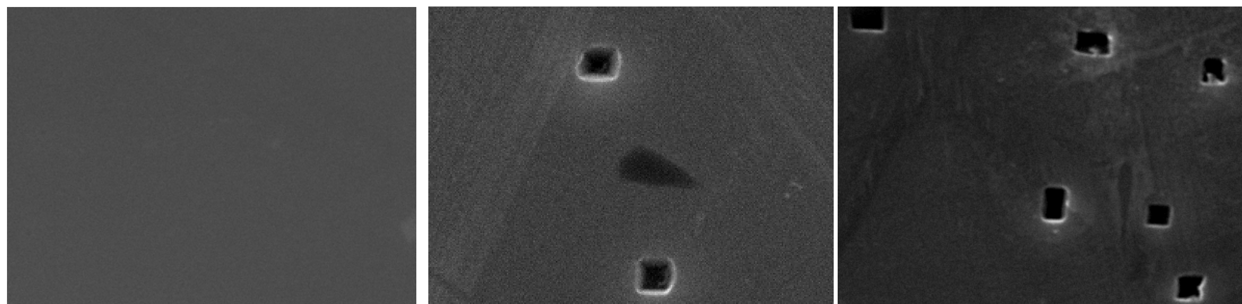

Figure 5. SEM micrographs of the etch-pits observed on Si surface in Cu/ALD-WC_xN_y(12 nm)/Si at (a) 550, (b) 600, and (c) 650 ºC.

CONCLUSIONS

We have investigated the film properties and the diffusion barrier performance of ALD-WN_xC_y film for Cu metallization. The as-deposited film showed a resistivity of about 350 μΩ-cm and density of 15.37 g/cm^3. The film composition showed a W, C, and N content of approximately 48, 32, and 20 at.%, respectively. The as-deposited film was composed of fcc β-WC_{1-x} or fcc β-W_2N from TEM analysis. The failure temperature of ALD-WN_xC_y diffusion barrier (12 nm) determined by XRD and sheet resistance measurements was 700 ^{o}C at 30 minutes annealing while the sputter-deposited Ta (12 nm) and ALD-TiN film (20 nm) failed after annealing at 650 and 600 ^{o}C, respectively. Our results show that ALD-WN_xC_y film can be considered as one of the viable candidates as the next generation diffusion barrier for Cu metallization.

ACKNOWLEDGEMENTS

Mrs. Jung-Hye Lee (KIST) is gratefully acknowledged for AES analysis. The authors (S.-H. Kim, S. S. Oh, and H.-M. Kim) are grateful to Brain Korea 21 scholarship by Ministry of Education, Korea. The assistance of Ki-Su Kim (Seoul National University) in depositing the Cu layer is greatly appreciated. The authors (S.-H. Kim, S. S. Oh, D.-H. Kang, H.-M. Kim, and K.-B. Kim) are members of Seoul National University Nanoelectronics Institute (SNI).

Table I. Performances of the barrier layers. The failure temperature is the annealing temperature where the copper silicide formation is first observed by XRD.

Sample	**Failure temperature (°C)**	**Annealing condition**	**Deposition notes**	Reference
Cu/WN_xC_y(12nm)/Si	**700**	**Vacuum 30 min**	**ALD using WF_6, NH_3, and TEB**	**This work**
Cu/TiN(10nm)/Si	500	Vacuum 30 min	Sputtering	19
Cu/TiN(28nm)/Si	550	H_2 1 hour	Thermal CVD using $TiCl_4$ and NH_3	20
Cu/TiN(19nm)/Si	650	H_2 1 hour	Plasma treated CVD using TDMAT[a]	
Cu/TiN(20nm)/Si	600	Vacuum 30 min	ALD using $TiCl_4$ and NH_3	This work
Cu/Ti(Al)N(10.6nm*)/Si	650	N_2 15 min	ALD using $TiCl_4$ NH_3, and TMA	21
Cu/TiC(50nm)/Si	650	N_2 30 min	Sputtering	22
Cu/Ta(12nm)	650	Vacuum 30 min	Sputtering	This work
Cu/TaN(25nm)/Si	800	5% H_2/N_2 120 min	Sputtering	23
Cu/TaN(50nm)/Si	600	Vacuum 30 min	Thermal CVD using PDEAT[b]	24
Cu/Ta(Al)N(10nm*)/Si	600	N_2 15 min	ALD using $TaCl_5$ NH_3, and TMA	8
Cu/$Ta_{48}C_{52}$(35nm)/Si	675	Vacuum 30 min	Sputtering	25
Cu/W(25nm)/Si	650	5% H_2/N_2 30 min	Sputtering	26
Cu/W_2N(8nm)/Si	700	5% H_2/N_2 30 min	Sputtering	
Cu/WC_x(50nm)/Si	700	N_2 30 min	Sputtering	27

*Film thickness was determined by energy dispersive spectroscopy (EDS) attached in SEM assuming the bulk density.

a and b denote tetrakis-dimethylamido-titanium and pentakis-diethylamido-tantalum, respectively.

REFERENCES

1. M. Leskelä and M. Ritala, Thin Solid Films **409**, 138 (2002).
2. T. Suntola, *Handbook of Crystal Growth* Vol. **3** Chapter 14, edited by D. T. J. Hurle, Elsevier Science B. V. (1994).
3. M. Ritala, M. Leskelä, E. Rauhala, and P. Haussalo, J. Elcecotrchem. Soc. **142**, 2731 (1995).
4. H. Jeon, J.-W. Lee, Y.-D. Kim, D.-S. Kim, and K.-S. Yi, J. Vac. Sci. Technol. A **18**, 1595 (2000).
5. K.-E. Elers, W. Saanila, P. J. Soininen, W.-M. Li, J. T. Kostamo, S. Haukka, J. Juhanoja, and W. F. A. Besling, Chem. Vap. Deposition **8**, 149 (2002).

6. M. Ritala, M. Leskelä, and J. Jokinen, J. Electrochem. Soc. **145**, 2914 (1998).
7. M. Ritala, P. Kalsi, D. Riihelä, K. Kukli, M. Leskelä, and J. Jokinen, Chem. Mater. **11**, 1712 (1999).
8. P. Alén, M. Juppo, M. Ritala, T. Sajavaara, J. Keinonen, and M. Leskelä, J. Electrochem. Soc. **148**, G566 (2001).
9. P. Alén, M. Juppo, M. Ritala, T. Sajavaara, J. Keinonen, and M. Leskelä, J. Mater. Res. **17**, 107 (2002).
10. J. W. Klaus, S. J. Ferro, and S. M. George, J. Electrochem. Soc. **147**, 1175 (2000).
11. J.-S. Park, H.-S. Park, and S.-W. Kang, J. Electochem. Soc. **149**, C28 (2002).
12. W.-M. Li, K.-E. Elers, J. Kostamo, S. Kaipio, H. Huotari, M. Soininen, P. J. Soininen, M. Tuominen, S. Haukka, S. Smith, and W. Besling, Proceedings of the IEEE 2002 International Interconnect Technology Conference, June 3-5, 2002, CA, pp.191.
13. S. Smith, W.-M. Li, K.-E. Elers and K. Pfeifer, Microelectronic Engineering **64**, 247 (2002).
14. L. R. Doolittle, Nucl. Instrum. Methods. Phys. Res. Sect. B **9**, 344 (1985).
15. S.-H. Kim, S. S. Oh, H.-M. Kim, D.-H. Kang, K.-B. Kim, W.-M. Li, S. Haukka, and M. Tuominen (Unpublished).
16. J.R. Tesmer, M. Nastasi, J.C. Barbour, C.J. Maggiore, and J.W. Mayer, *Handbook of Modern Ion Beam Materials Analysis*, Materials Research Society (1995).
17. K.-C. Park, K.-B. Kim, I. Raaijmakers, and K. Ngan, J. Appl. Phys. **80**, 5674 (1996).
18. C. Cabral Jr., C. Lavoie, J.M.E. Harper, and J. Jordan-Sweet, Thin Solid Films **397**, 194 (2001).
19. K. T. Nam, A. Datta, S.-H. Kim, and K.-B. Kim, Appl. Phys. Lett. **79**, 2549 (2001).
20. S.-H. Kim, D.-S. Chung, K.-C. Park, K.-B. Kim, and S.-H. Min, J. Electrochem. Soc. **146**, 1455 (1999).
21. M. Juppo, P. Alén, M. Ritala, and M. Leskelä, Chem. Vap. Deposition. **7**, 211 (2001).
22. S. J. Wang, H. Y. Tsai, and S. C. Sun, J. Electrochem. Soc. **148**, C563 (2001).
23. T. Oku, E. Kawakami, M. Uekubo, K. Takahiro, S. Yamaguchi, M. Murakami, Appl. Surf. Sci. **99**, 265 (1996).
24. S.-H. Kim, S.-J. Im, and K.-B. Kim, Thin Solid Films **415**, 177 (2002).
25. T. Laurila, K. Zeng, J. K. Kivilahti, J. Molarius, and I. Suni, J. Appl. Phys. **91**, 5391 (2002).
26. M. Uekubo, T. Oku, K. Nii, M. Murakami, K. Takahiro, S. Ymaguchi, T Nakano, and T. Ohta, Thin Solid Films **286**, 170 (1996).
27. S. J. Wang, H. Y. Tsai, S. C. Sun, and M. H. Shiao, J. Electrochem. Soc. **148**, G500 (2001).